Hysteresis effects of suspended sediment transport in relation to geomorphic conditions and dominant sediment sources in medium and large rivers of the Russian Arctic

Nikita I. Tananaev

ABSTRACT

Preliminary analysis of long-term hydrological data shows that sediment dynamics of Russian Arctic rivers is largely affected by hysteresis effects in relation of water discharge to suspended sediment concentration (SSC). The role of large-scale geomorphic and geocryological conditions in sediment transport is still relatively understudied. This research aims to assess the links between hydrogeomorphology and regularities of sediment formation and movement in Russian Arctic rivers. A dataset containing information on measured water discharges and SSC for 27 gauges on 16 medium and large rivers of the Russian Arctic was used in this research. Clockwise hysteresis is typical during spring events, while in summer counterclockwise and 'figure eight' curves are widely observed. The results show that the form of the rating curve can be attributed to the dominant sediment source, dominant channel pattern and, to certain extent, to the cross-section position within the river basin. Seasonality in hysteresis effects reflects the role frozen ground dynamic plays in sediment flux formation. Thus, reaction of permafrost landscapes on the widely observed climate shift should lead to significant changes in sediment transfer systems.

Key words | Arctic hydrology, hysteresis effects, sediment sources, suspended sediment rating curves

Nikita I. Tananaev
Permafrost Institute,
Siberian Division,
Russian Academy of Science,
Bldg. 8A,
1-st District,
Igarka,
Krasnoyarsk Region,
Russia
E-mail: *nikita.tananaev@gmail.com*

INTRODUCTION

Perspectives of Arctic development draw attention to all characteristics of the region's ecosystems, including hydrogeomorphic features and associated sediment fluxes. Sediment-related water use issues are well known and include, but are not limited to, higher costs of water intake and conditioning (Konrad *et al.* 2006), reservoir siltation, water quality loss and aquatic ecosystem degradation, associated chemical fluxes and river navigation issues (Bash *et al.* 2001; Taylor *et al.* 2008; Viers *et al.* 2009). Quantitative characteristics of suspended sediment load should be taken into account while developing land use schemes for river valleys and channel sections, construction and hydraulic engineering projects. Continued attention to recent climate shifts in the Arctic adds to the rising interest in detailed studies of contemporary sediment dynamics within the catchments of the region. The inadequate level of detail in these studies is primarily attributed to sparse gauging networks and the lack of long-term series of monitoring data.

Suspended sediment concentration (SSC) is extensively used in sediment load calculations, the latter being frequently carried out using a well-established method of relating water discharge to SSC, the so-called 'sediment rating curve' (Campbell & Bauder 1940; Walling 1977):

$$\mathrm{SSC} = aQ^b, \tag{1}$$

where SSC is suspended sediment concentration (measured), $\mathrm{g\,m^{-3}}$, Q is corresponding water discharge, $\mathrm{m^3\,s^{-1}}$, a and b are empirical rating curve coefficients. Combination of

doi: 10.2166/nh.2013.199

rating curve coefficients reflects the intensity of geomorphic response to variable hydrological conditions, and is correlated with major physiographic features of the watersheds (Rannie 1978; Mimikou 1982; Syvitski *et al.* 2000; Tananaev 2007a, b). Rating curves can be developed using data of variable temporal resolution, from measured to annual, but for most applications, observation data or daily averages are used. Heteroscedasticity of model residuals for nonlinear regression models (Equation (1)) can lead to the significant miscalculations of sediment loads (Walling 1977; Ferguson 1986; Balamurugan 1989). Variations of water discharge and SSC values, either due to climatic variability, seasonal changes in erosion intensity or river transport capacity, lead to the high level of uncertainty in deriving the rating curve centreline. The resulting 'scatter cloud' generally reflects the hysteresis effects in water discharge vs. SSC relationship, when SSC values can be highly variable at constant discharge values (Asselman 1999). Splitting the SSC data by the rising or falling stage of the single hydrological event and plotting the individual rating curve for each stage leads to a significant increase in sediment load estimation quality (Walling & Webb 1982; Aquino *et al*. 2009).

The aim of this study was to outline the general features of temporal variations in suspended sediment fluxes of Russian Arctic rivers and assess the role that hydrogeomorphic conditions play in suspended sediment flux origin. Understanding the geomorphic nature of hysteresis effect, its relation to sediment system dynamics should improve the effectiveness of sediment yield estimations and allow better predictions for the ungauged Arctic basins.

SSC VS. WATER DISCHARGE HYSTERESIS

During single hydrological events, hysteresis effect occurs when SSC values on the rising limb of the hydrograph differ from those of the falling limb for the same discharges. Positive (or clockwise) hysteresis occurs if rising limb SSC values exceed that of the falling limb, otherwise negative (or counterclockwise) hysteresis is observed (Williams 1989). The effect is generally attributed to the changes in sediment availability throughout the event, when these peaks are synchronous, but also to the time shift between water discharge and SSC peaks (Bača 2008).

Clockwise (positive) hysteresis can be attributed to earlier SSC peak occurrence, either due to SSC increase at the earlier stage of the event or rapid SSC decline at the latter stages, before the discharge peak. Sediment wave is supposed to move ahead of discharge wave, since, following the Airy relation, it is associated with the highest stream velocity, which occurs before the discharge peak (Arnborg *et al.* 1967). A sharp SSC peak is also observed when sediment source is adjacent to the measurement site and is exhausted during the event (Asselman 1999). Highly sorted channel alluvium, accumulated during the previous event, appears to be the most accessible sediment source (Bogen 1980; Bača 2008). The decline in SSC is generally caused by overall sediment source exhaustion during the event, limiting sediment supply to the stream (Peart & Walling 1988; Slattery *et al.* 2002; Bača 2008). When flow transport capacity is not 'detached' from the sediment sources, stormflow dilution by base flow can affect the SSC values at any event phase (Wood 1977). This allows application of a simplified mixing model to SSC prediction during single events (Walling & Webb 1982). Other reasons for SSC decline include decreasing rain intensity and droplet erosion energy at the latter stages of the event (Rodriguez-Blanco *et al.* 2010a), rill and gully erosion ceasing or detachment from stream (diCenzo & Luk 1997; Rodriguez-Blanco *et al.* 2010b), 'armour layer' formation in the channel (Kleinhans *et al*. 2007) and post-collapse bank reinforcement with turf and root systems (Arnborg *et al.* 1967).

Counterclockwise (negative) hysteresis occurs due to intensive SSC increase subsequent to the discharge peak. This case is relatively rarely observed. Asynchronous response from the watershed and delayed sediment waves from the distant tributaries are considered as major causes for negative hysteresis (Walling & Webb 1982; Bača 2008). According to Kleinhans *et al.* (2007), armour layer detachment at peak discharges can initiate underlying alluvium particle movement at the falling limb of the event. The frozen state of the catchment surface may be responsible for negative hysteresis effect in permafrost-affected areas due to soil and gully erosion offset until the active layer has been developed (Tananaev 2009). Unrelated to flow conditions, SSC peaks originating from rapid mass movement

episodes (solifluction, thermoerosional niche failures, cryogenic debris, etc.) during the falling stage may also produce counterclockwise hysteresis (Arnborg *et al.* 1967; Irvine-Fynn *et al.* 2005; Lewis *et al.* 2005).

Thus, hysteresis effects in sediment dynamics appear to be linked closely with the geomorphic conditions within the watersheds. Furthermore, appearance of the rating curve is sometimes indicative of dominant sediment sources (Peart & Walling 1988). Positive curves relate to overall sediment source depletion during the event, while negative hysteresis is connected to rapid and highly localized mass movement episodes (bank failure, retrogressive thaw slumps and active layer detachment slides). It is worth noting that previous studies mostly discuss data on small streams and catchments in moderate humid climates. Sediment fluxes from Arctic watersheds are still poorly described, reflecting the absence of long-term datasets and sparse gauging networks. The latter also undermines the efforts of large-scale geographical generalization of the phenomenon, which is essential for developing adequate suspended sediment load prediction techniques for ungauged basins.

MATERIALS AND METHODS

Establishing rating curves requires long-term data on measured values of both water discharges and SSC. Data quality, in terms of both observations of duration and number of measurements, is highest for the largest rivers. In this study, a dataset containing measured SSC and water discharge values for 27 gauging stations on 16 rivers of the Russian Arctic was employed (Figure 1). These stations are part of the state observational network and run under standard procedures and data collection protocols. The dataset, therefore, has a high degree of internal consistency in terms of employed techniques and instrumentation.

Water discharge was measured at random time intervals, to cover the full range of water stage variability and construct a reliable stage–discharge relationship. Measurements followed the standard procedures, including multipoint velocity observations with the propeller, and discharge calculations using 'velocity-area' technique. SSC samples were collected at random time intervals, depending on the discharge. During the first years of gauging operations, samples were collected both at multiple points throughout the cross-section and at a single-point location near the middle of the river, in order to obtain a stable relation between cross-sectional average and single-point SSC values. Later on, only single-point sampling was carried out. Samples were collected manually using a standard bathometer. SSC was later calculated gravimetrically by filtration through pre-weighted paper filters ('white stripe'). Filters were further dried at 105 °C for 2 hours and weighted on the analytical balance with an accuracy of 0.001 g. Estimated average observation error is below 5% for water

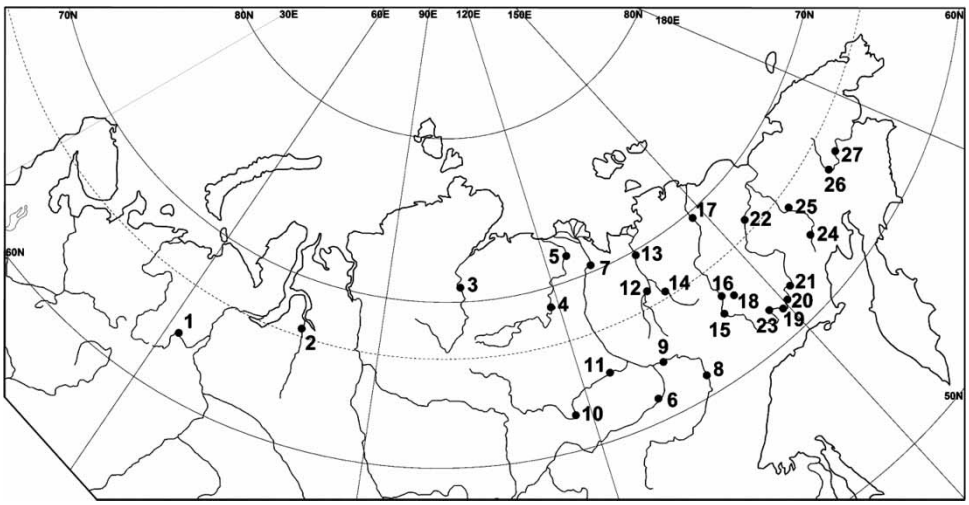

Figure 1 | Study region scheme. Gauging station numbers correspond to those in Tables 1 and 3.

discharge measurements and around 20–25% for SSC measurements.

Rivers included in the dataset are among the largest in the region, but vary significantly in terms of both basin area (from 3,700 to 2,400,000 km^2) and mean annual discharge (from 40 to 16,500 $m^3 s^{-1}$) (Table 1). Gauging stations are spread over the vast territory of Western and Eastern Siberia, and the catchments of the studied rivers integrate the response of diverse landscapes of the Russian Arctic. Tundra landscapes with shallow active layer and icy low-temperature permafrost are typical for the areas above the Arctic Circle, adjacent to the Arctic Ocean

Table 1 | General features of 27 gauging stations of the Russian Arctic, included in the dataset (aggregated from R-Arctic database (Lammers *et al*. 2001))

No.	Gauging station	Latitude, °N	Longitude, °E	Gauge height, m	Area, km^2	Q, $m^3 s^{-1}$
Kara Sea basin						
1	Severnaya Sos'va at Sos'va	63.65	62.10	12.04	65,200	612
2	Pur at Samburg	67.00	78.22	−2.12	91,500	892
Laptev Sea basin (westwards from Lena delta)						
3	Anabar at Saskylakh	71.97	114.08	3.45	78,800	453
4	Olenek at Sukhana	68.62	118.33	44.45	127,000	715
5	Olenek at 7.5 km down Buur mouth	71.85	123.65	−1.31	181,000	1,170
Laptev Sea basin (Lena River and tributaries)						
6	Lena at Tabaga	61.83	129.60	85.08	897,000	7,010
7	Lena at Kyusyur	70.68	127.39	−1.41	2,430 000	16,800
8	Aldan at Okhotsky Perevoz	61.87	135.50	125.28	514,000	4,240
9	Aldan at Verkhoyansky Perevoz	63.32	132.02	74.1	696,000	5,260
10	Viluy at Suntar	62.15	117.65	109.35	202,000	788
11	Viluy at Khatyryk-Khomo	63.95	124.83	64.44	452,000	1,480
Laptev Sea basin (eastwards from Lena delta)						
12	Yana at Verkhoyansk	67.37	133.38	124.91	45,300	155
13	Yana at Dzhangky	69.77	135.23	36.2	216,000	927
14	Adycha at Oyun-Khomoto	67.33	135.60	148.99	65,500	328
East-Siberian Sea basin						
15	Indigirka at Yurty	64.05	141.88	578.11	51,100	236
16	Indigirka at Indigirsky	64.53	143.12	482.01	83,500	422
17	Indigirka at Vorontsovo	69.57	147.53	3.41	305,000	1,590
18	Nera at Ala-Chubuk	64.43	144.37	568.25	22,300	119
19	Kolyma at Duskanya	61.65	148.83	426.95	50,100	334
20	Kolyma at Sinegor'ye	62.07	150.47	327.17	61,500	458
21	Kolyma at Ust'-Srednekan	62.43	152.30	221.9	99,400	728
22	Kolyma at Srednekolymsk	67.47	153.69	8	361,000	2,200
23	Ayan-Uryakh at Emtegey	62.83	146.62	644.54	9,560	66.7
24	Omolon at Omolon (Labaznaya)	63.32	158.43	696.17	3,710	37.9
25	Oloy at Utochan	65.67	162.43	367.37	15,700	113
Bering Sea basin						
26	Anadyr at Novy Yeropol	64.83	168.75	85.85	47,300	473
27	Anadyr at Snezhny	65.45	172.97	1.21	106,000	992

coastline. The Verkhoyansk Range, spreading along the right side of the Lena River valley in its middle and lower sections, is the natural border that separates plains and plateaus of Eastern Siberia from the Verkhoyansk-Kolyma mountainous region of North-Eastern Russia.

Measured water discharge and SSC data, accumulated in this dataset, were officially published by the Russian Hydrometeorological Agency during the period 1956–1986. After 1986, measured SSC values were excluded from official publications, and were substituted by 10-day SSC averages, which were not used in this study. Data availability and level of detail in terms of both observation period length and number of measurements (SSC–discharge pairs) varies through the dataset (Table 2). The least data availability is for the Kolyma basin (40–60 measurements, 3–7 years of record), while the highest is for the Indigirka basin (150–219 measurements, 12–17 years of record). The majority of field observations were conducted during ice-free periods. Since mostly data for the falling limb of the spring events are present in the published materials, it was hardly possible to plot individual curves for such events for many stations and years.

Since strict quantitative methods of rating curve analysis are still to be developed, simple plotted data analysis was employed to outline hysteresis effect features. The relative peak position of SSC and discharge, skewness and width of the curves are highly illustrative in these terms. Qualitative typology of SSC–discharge plots, described by Williams (1989), was used in this study. Following Williams (1989), curves were categorized into five classes, each containing from one to four types (Table 3). Additional data regarding suspended sediment flux features were used where possible to emphasize the impact of hydrogeomorphic conditions.

RESULTS AND DISCUSSION

Time resolution of the observation does not allow revealing high-frequency SSC variations, as average time shift between individual samplings exceeds 3–4 days. Thus, this study describes only general features of the SSC temporal dynamics. From the available dataset, records for over 500 spring and summer–autumn flood events were derived. Spring events are generated by snowmelt, while summer and autumn floods correspond to rainfall events. For the large part of the events, available data were insufficient to obtain a reliable SSC–discharge graph. Only 330 individual graphs were reviewed in the scope of the study. Produced hysteresis plots were classified following detailed SSC–discharge curves typology, developed by Williams (1989). Different types of Class II (clockwise loop) and III (counterclockwise loop) curves dominate the dataset, with Class V ('figure eight' loop) observed frequently, especially during summer and autumn events (see Table 2).

Hysteresis effects during spring events

Throughout the studied region, SSC generally rises with discharge during spring events, and positive hysteresis is observed (Figures 2(a) and 2(b)). A major source of suspended particles during spring floods is channel alluvium, because continuous permafrost extent limits the catchment source activity. When suspended sediments originate from distant sources, the SSC peak is generally observed 3–5 days prior to the discharge peak (Type II*a*), since turbidity wave moves through the fluvial network faster than discharge wave (Arnborg *et al.* 1967). When channel alluvium sources are located close to the gauge station, SSC and discharge peaks are nearly synchronous (Type II*b*). This curve type is frequently observed in rivers with braided channels (Tananaev 2009), a fact which underlines the role of alluvial sand bars as sediment source areas.

Asymmetrical hysteresis loops are formed when SSC and Q graphs differ in increase or decrease rates, and their peaks are asynchronous (Williams 1989). Sharp SSC peak preceding Q maximum forms Type II*c* loops (Figure 2(c)), which are common for mountainous rivers of the East-Siberian Sea basin. Relative position and form of the peaks evidence a short-term, pulse sediment input into the stream with following sharp source exhaustion. While surface and bank erosion in spring is strictly limited due to permafrost presence, sediment flux at that time is probably associated with resuspension of channel alluvium, deposited during autumn and winter of the preceding year. This channel material is fine-grained, highly sorted and easily available for stream erosion (Bogen 1980). During the event, fine-grained sediment sources are rapidly exhausted,

Table 2 | Major types of SSC-discharge rating curves on rivers of Russian Arctic; curve types given following typology of Williams (1989)

				Dominant rating curve type[a]	
No.	**Gauging station**	**No. of observations**	**Years of record**	**Spring**	**Summer–autumn**
Kara Sea basin					
1	Severnaya Sos'va at Sos'va	162	12	$\frac{\text{II}a - \text{II}b}{8 - 4(12)}$	$\frac{\text{II}a - \text{III}a}{6 - 3(11)}$
2	Pur at Samburg	275	20	$\frac{\text{II}d}{3(15)}$	$\frac{\text{II}d}{4(4)}$
Laptev Sea basin (westwards from Lena delta)					
3	Anabar at Saskylakh	49	7	–[b]	$\frac{\text{III}b - \text{V}}{2 - 1(3)}$
4	Olenek at Sukhana	134	14	$\frac{\text{II}c - \text{II}b}{6 - 3(9)}$	$\frac{\text{II}c - \text{III}b}{4 - 3(8)}$
5	Olenek at 7.5 km down Buur mouth	257	10	$\frac{\text{II}c - \text{V}a}{5 - 4(9)}$	$\frac{\text{II}d - \text{V}}{4 - 3(10)}$
Laptev Sea basin (Lena River and tributaries)					
6	Lena at Tabaga	195	19	$\frac{\text{II}b - \text{II}c}{7 - 6(13)}$	$\frac{\text{II}b - \text{II}c}{7 - 3(13)}$
7	Lena at Kyusyur	71	11	$\frac{\text{V} - \text{III}b}{4 - 3(9)}$	–[b]
8	Aldan at Okhotsky Perevoz	76	4	$\frac{\text{II}a - \text{II}b}{2 - 2(4)}$	$\frac{\text{III}b - \text{V}}{5 - 2(7)}$
9	Aldan at Verkhoyansky Perevoz	61	6	$\frac{\text{II}b}{4(5)}$	$\frac{\text{II}b - \text{V}}{2 - 2(5)}$
10	Viluy at Suntar	240	12	$\frac{\text{II}d - \text{II}a}{7 - 4(12)}$	$\frac{\text{V}}{6(10)}$
11	Viluy at Khatyryk-Khomo	95	10	$\frac{\text{II}d - \text{II}b}{2 - 2(6)}$	–[b]
Laptev Sea basin (eastwards from Lena delta)					
12	Yana at Verkhoyansk	249	11	$\frac{\text{II}c - \text{V}}{5 - 4(10)}$	$\frac{\text{II}b - \text{II}c}{4 - 4(12)}$
13	Yana at Dzhangky	63	6	$\frac{\text{III}b - \text{V}}{2 - 1(3)}$	$\frac{\text{V}}{2(4)}$
14	Adycha at Oyun-Khomoto	212	11	$\frac{\text{II}b - \text{V}}{5 - 2(9)}$	$\frac{\text{III}b - \text{V}}{6 - 2(10)}$
East-Siberian Sea basin					
15	Indigirka at Yurty	150	12	$\frac{\text{II}c - \text{III}b}{4 - 2(9)}$	$\frac{\text{II}b - \text{V}}{5 - 3(9)}$
16	Indigirka at Indigirsky	183	13	$\frac{\text{II}b - \text{III}a}{6 - 3(9)}$	$\frac{\text{II}b - \text{V}}{9 - 4(16)}$
17	Indigirka at Vorontsovo	219	17	$\frac{\text{II}c - \text{III}a}{6 - 3(10)}$	$\frac{\text{II}c - \text{III}b}{7 - 4(11)}$
18	Nera at Ala-Chubuk	99	11	$\frac{\text{II}b - \text{III}b}{5 - 2(7)}$	$\frac{\text{III}b - \text{V}}{4 - 2(6)}$
19	Kolyma at Duskanya	55	3	$\frac{\text{II}c}{3(3)}$	$\frac{\text{II}c}{2(2)}$

(*continued*)

Table 2 | continued

No.	Gauging station	No. of observations	Years of record	Dominant rating curve type[a]	
				Spring	Summer–autumn
20	Kolyma at Sinegor'e	44	2	IIc 2(2)	IIc 4(5)
21	Kolyma at Ust'-Srednekan	63	8	IIc 6(6)	V 5(2)
22	Kolyma at Srednekolymsk	40	7	IIc – V 3 – 2(5)	IIIb – V 2 – 1(3)
23	Ayan-Uryakh at Emtegey	161	12	IIa – Iid 5 – 3(9)	IIc – V 6 – 3(11)
24	Omolon at Omolon (Labaznaya)	40	4	IIc 3(3)	IIc – V 1 – 1(2)
25	Oloy at Utochan	19	1	IIc n/a	V n/a
Bering Sea basin					
26	Anadyr at Novy Yeropol	40	2	IIb 2(2)	–[b]
27	Anadyr at Snezhny	128	8	IIb 6(7)	IIIb – V 3 – 1(4)

[a]Dominant curve types are given in divisor, and number of events, corresponding to those types, in denominator; total number of events is given in parentheses.
[b]Data are missing or insufficient.

Table 3 | Typology of SSC-discharge plots, described by Williams (1989)

Class	Type and description
I. Single-valued line	a. Straight line b. Bending upward line c. Bending downward line
II. Clockwise loop	a. SSC peaking before discharge b. Simultaneous peaks of SSC and discharge; asymmetrical SSC and discharge peaks c. Spread of SSC graph less than that of discharge graph; bending upwards loop d. Spread of SSC graph greater than that of discharge graph; bending rightwards loop
III. Counterclockwise loop	a. SSC peaking after discharge b. Same as II*b* – counterclockwise direction c. Same as II*c* – counterclockwise direction d. Same as II*d* – counterclockwise direction
IV. Single line plus a loop	Highly asymmetrical SSC graph, peaking ahead of discharge
V. Figure eight	SSC and discharge graphs of variable skewness

and stream starts eroding channel-forming alluvium, which is normally much coarser. The latter leads to sharp SSC decrease even with increasing water discharges.

Analysis of grain-size data, published in Russian Hydrometeorological Agency Hydrological yearbooks, shows agreement with the results, previously published by Arnborg *et al.* (1967) and Kleinhans *et al.* (2007), and several examples are given below. For example, during the falling limb of 1960 spring flood event (Adycha at Oyun-Khomoto), average grain-size increased almost twice, from 0.13 to 0.24 mm, due to an increase in percentage of particles coarser than 0.05 mm (from 26.3 to 38.7%). During the 1967 spring flood (Indigirka at Vorontsovo), a sharp increase of 0.1–0.2 mm particle content was observed (from 0.5 to 27.7%), with a total increase in percentage of particles coarser than 0.05 mm (from 30.1 to 55.3%). A sharp decrease in channel sediment supply can also be attributed to the presence of a within-channel permafrost layer, limiting river bed deformations until degraded due to heat exchange with stream flow (Tananaev 2007a, b).

Extended SSC wave, sometimes passing ahead of discharge wave, forms Type II*d* loops (Figure 2(d)). It is

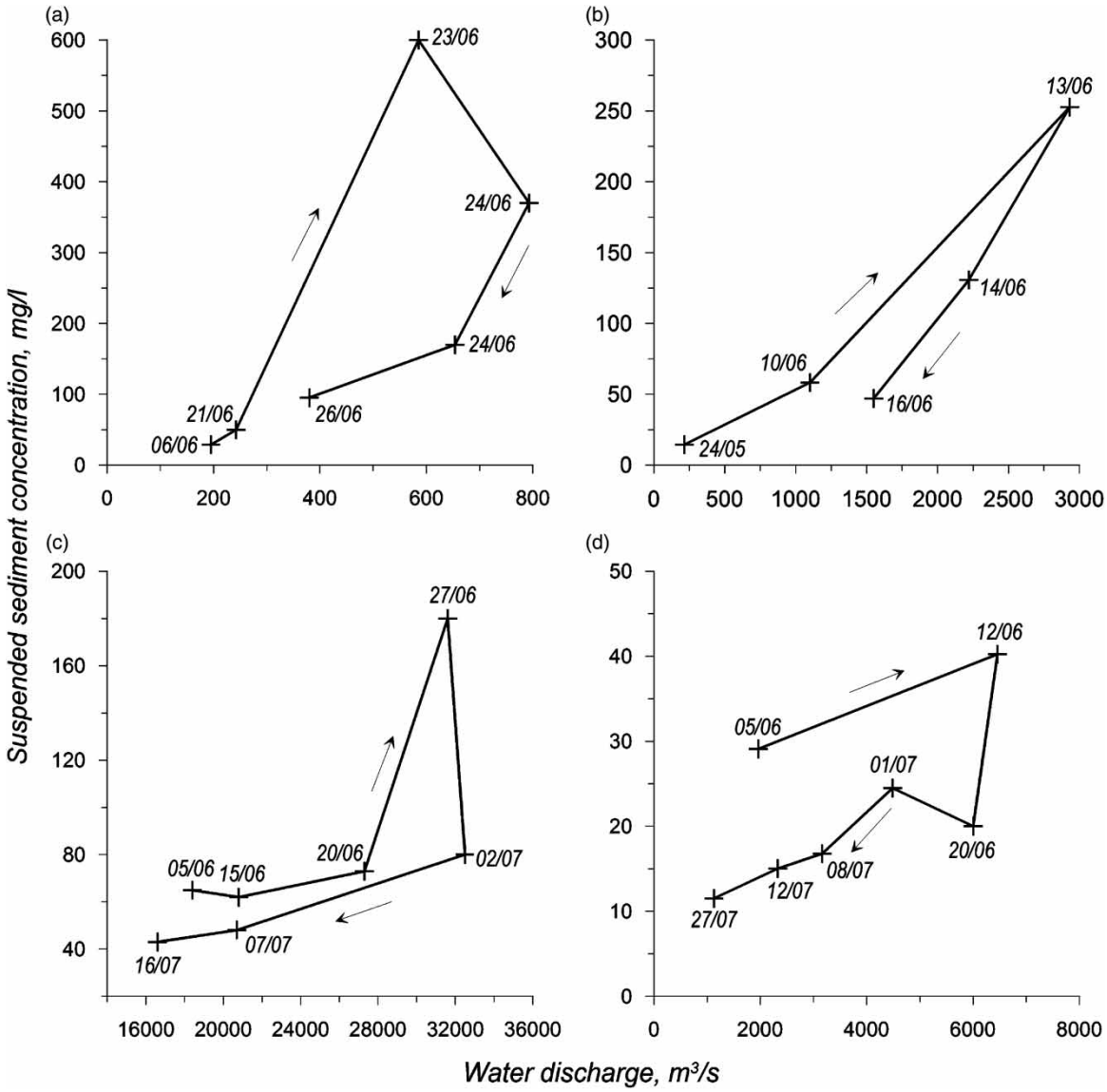

Figure 2 | Positive hysteresis graph examples: (a) Type II*a*, Ayan-Uryakh at Emtegey, 1972; (b) Type II*b*, Indigirka at Indigirsky, 1960; (c) Type II*c*, Lena at Tabaga, 1964; (d) Type II*d*, Pur at Samburg, 1959.

observed during spring events on the rivers Pur and Viluy, and is characterized by relatively low SSC values. This is attributed to baseflow dilution during falling stage of the event, with surface erosion and sediment delivery limited by high wetland coverage (Pur river basin) and channel deformations restricted by within-channel permafrost (Viluy river).

Counterclockwise hysteresis loops (Type III*a* and III*b*; Figure 3) are uncommon during spring floods, and are observed only on rivers of North-Eastern Russia (Yana, Indigirka and their tributaries), situated in the most harsh climatic and geocryological conditions. During winter freezing, river cross-sections are often fully closed with ice, thus stream only exists as a sub-channel flow. This leads to a sharp increase of moisture content in fine-grained channel sediment (loam and sandy loam), leading to formation of within-channel permafrost lenses with extremely high ice content (Van Vliet-Lanoë *et al.* 1984). Channel sediment supply during spring events in such conditions is reduced

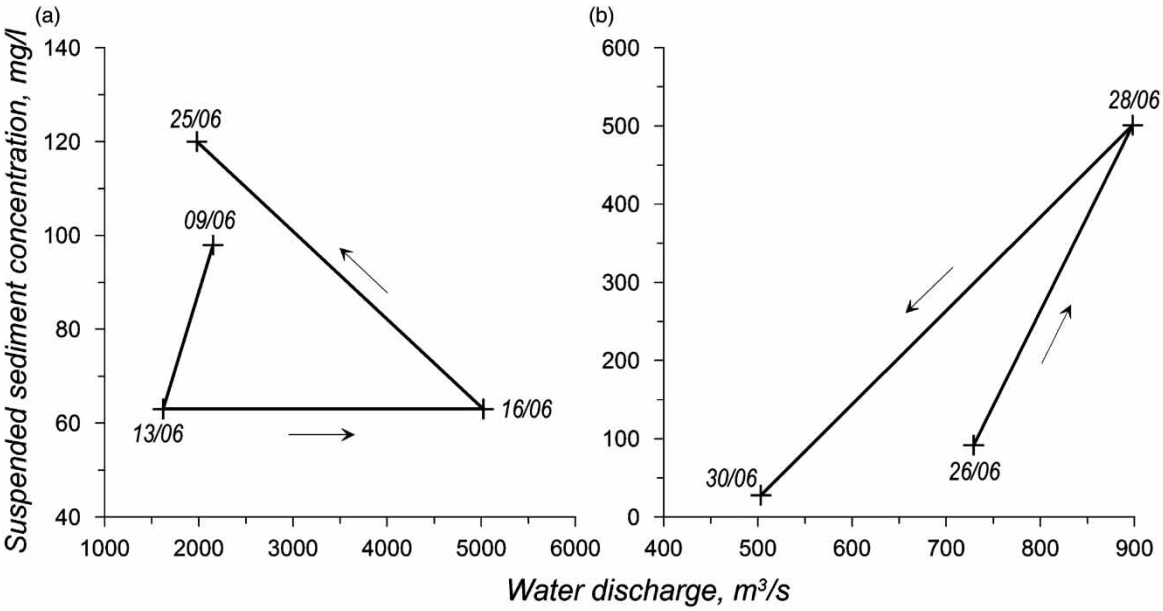

Figure 3 | Negative hysteresis graph examples: (a) Type III*a*, Yana at Dzhangky, 1973; (b) Type III*b*, Nera at Ala-Chubuk, 1967.

to minimum and SSC peaks are formed during late stages of the spring events due to activization of surface erosion and thermoerosional bank failure.

Overlapping input from several sediment sources or tributaries, generally independent from water regime on gauge station, leads to asynchronous plot looping, so-called 'figure eight' (Figure 4). In the studied region, highly affected by permafrost dynamics, such loops are generated by consecutive sediment waves linked with resuspended alluvium, asynchronous input from tributaries. During the later stages of the event, sheet and gully erosion, as well as bank collapse, supply sediment to the channel.

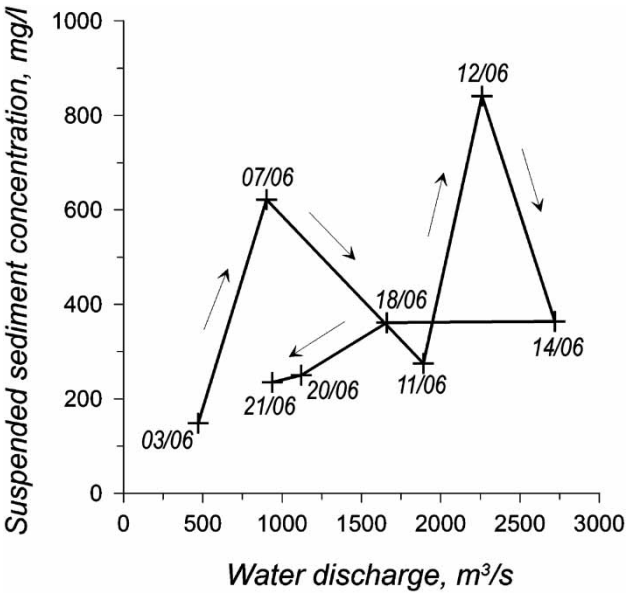

Figure 4 | 'Figure eight' (Type V) hysteresis graph example: Yana at Verkhoyansk, 1967.

Hysteresis effects during summer–autumn events

A strongly pronounced summer–autumn flood period is present in the water regime of all studied rivers. The average number of flood events varies throughout the region, from two to three events on North-Siberian rivers (westwards from the Verkhoyansk Range) up to four to eight events on rivers of North-Eastern Russia (westwards from the Verkhoyansk Range). Some events on rivers with a flood-dominated water regime can have water discharges much higher than those that are observed during spring events.

A positive hysteresis effect during summer and autumn flood events is observed in two diverse physiographic areas – in the north of Western Siberia and on rivers of the Verkhoyansk-Kolyma Mountainous region. In Western Siberia, sediment input from surface erosion stays relatively low due to high wetland and lake

coverage, high turf content in river banks, while channel sources are rapidly exhausted during the event (especially during the series of consequent events). In mountainous areas of North-Eastern Russia, positive hysteresis effects are predominantly linked with the intensive supply from groundwater and aufeis melting, adding to the dilution of stormflow (Walling & Webb 1982). Dilution effects play the major role during subsequent flood events, when extremely high moisture content above the permafrost table leads to intensification of surface flow. Surface erosion and active mass movement processes in mountainous areas deliver to the streams mostly coarse particles, which are transported further as bed load.

Negative hysteresis loops are widely observed throughout the region, and are the most common rating curve type on gauge stations that are situated in transitional channel segments, where rivers leave mountainous regions and enter large alluvial plains (gauging stations 8, 14, 22, 27 in Figure 1, Tables 1 and 2). The counterclockwise hysteresis effect here can be attributed to difference in localization of discharge and SSC peak origin. A discharge peak is formed in the mountainous part of the watershed, while dominant sediment sources are situated in piedmont areas and, sometimes, within plains. As a result, sediment-free stormflow wave passes through the cross-section before the sediment wave is generated in piedmont locations, thus forming negative rating curves. Active bank retreat and active gully erosion within floodplains add to the SSC increase at the latter stages of the events.

Chaotic rating curve, which can be described as 'figure eight', but frequently having a more complex form, is the dominating rating curve type during summer–autumn flood events in lower reaches of the studied rivers (gauging stations 3, 5, 9, 13 in Figure 1, Tables 1 and 2). This is also frequently observed in mountainous catchments with lower response time to rainfall events (gauging stations 14–16, 21, 23, 24 in Figure 1, Tables 1 and 2). For each studied cross-section an individual combination of sediment sources and delivery processes exist for each year and single event, adding to the complexity of observed rating curves. Pulse inputs from bank failure, other mass movement episodes, can superimpose sediment waves coming from tributaries or channel sources, forming SSC peaks above the background values.

CONCLUSION

Hysteresis effects in relations between water discharge and SSC appear to be common sediment dynamics features of Russian Arctic rivers. Major factors, leading to nonlinearity and variability in this relationship, include seasonal variations in sediment sources, rates of discharge and SSC wave movement, asynchronous feedback from different elements of fluvial systems during single flood events. Drivers for these factors include regional diversity of water regime patterns and active layer dynamics.

Positive hysteresis is observed during spring high-flow on most of the studied rivers. As sediment load majorly originates from channel sources, easily available but also rapidly exhaustible, a SSC wave normally precedes water discharge peak. Event flow dilution by baseflow takes place on rivers of Western Siberia, having relatively higher wetland and lake extent within their watersheds. Negative loops in spring are generally observed in North-Eastern Russia, either due to extremely low SSC values at the rising limb of the hydrograph (when major sediment sources are detached from the streams) or high SSC values at the falling limb (when mass movement processes occur within the active layer). In Arctic environments, within-channel sediment sources are likely to play a major role during spring events, when surface erosion is inactive due to high snow cover extent.

During summer and autumn flood events, stormflow dilution by baseflow and exhaustion of channel sediment sources lead to clockwise hysteresis, while asynchronous reaction of mountainous and piedmont channel reaches on storm events and active bank retreat induce counterclockwise hysteresis to occur. Positive curve types relate to basins where watershed erosion is limited either due to wetland or lake extent or where groundwater and aufeis play significant roles as water sources.

Results underscore the role permafrost plays in Arctic environments in relation to sediment flux formation. It appears to limit sediment supply from both watersheds and river channels during spring events, but enhances

erosivity and watershed-channel coupling during summer and autumn events.

ACKNOWLEDGEMENT

This study was carried out under Russian Academy of Science 2008–2012 Basic Research Program, Project VII.63.2.4.

REFERENCES

Aquino, S., Latrubesse, E. M. & Bayer, M. 2009 Assessment of wash load transport in the Araguaia River (Aruana gauge station). *Lat. Am. J. Sedimentol. Basin Anal.* **16** (2), 119–128.

Arnborg, L., Walker, H. J. & Peippo, J. 1967 Suspended load in the Colville river, Alaska, 1962. *Geografiska Annaler, Series A* **49** (2/4), 131–144.

Asselman, N. E. M. 1999 Suspended sediment dynamics in a large basin: the river Rhine. *Hydrol. Process.* **13**, 1437–1450.

Bača, P. 2008 Hysteresis effect in suspended sediment concentration in the Rybárik basin, Slovakia. *Hydrol. Sci. J.* **53** (1), 224–235.

Balamurugan, G. 1989 The use of suspended sediment rating curves in Malaysia: some preliminary considerations. *Pertanika* **12** (3), 367–376.

Bash, J., Berman, C. & Bolton, S. 2001 *Effects of Turbidity and Suspended Solids on Salmonids*. University of Washington, Center for Streamside Studies, Research Project T1803, Task 42, Seattle, WA, p. 74.

Bogen, J. 1980 The hysteresis effect of sediment transport system. *Norwegian J. Geogr.* **34** (1), 45–54.

Campbell, F. B. & Bauder, H. A. 1940 A rating-curve method for determining silt discharge in streams. *AGU EOS Trans.* **21**, 603–607.

diCenzo, P. D. & Luk, S. 1997 Gully erosion and sediment transport in a small subtropical catchment, South China. *Catena* **29**, 161–176.

Ferguson, R. I. 1986 River loads underestimated by rating curves. *Water Resour. Res.* **22** (1), 74–76.

Irvine-Fynn, T. D. L., Moorman, B. J., Willis, I. C., Sjogren, D. B., Hodson, A. J., Mumford, P. N., Walter, F. S. A. & Williams, J. L. M. 2005 Geocryological processes linked to High Arctic proglacial stream suspended sediment dynamics: examples from Bylot Island, Nunavut, and Spitsbergen, Svalbard. *Hydrol. Process.* **19**, 115–135.

Kleinhans, M. G., Wilbers, A. W. E. & ten Brinke, W. B. M. 2007 Opposite hysteresis of sand and gravel transport upstream and downstream of a bifurcation during a flood in the river Rhine, the Netherlands. *Neth. J. Geosci.* **86** (3), 273–285.

Konrad, C., Pottsmith, C., Melis, T. & Rubin, D. 2006 Real-time analysis of concentrated fluvial suspended sediment. In: *Proc. 8th Federal Interagency Sedimentation Conference*, Reno, Nevada, 2006, pp. 585–591.

Lammers, R. B., Shiklomanov, A. I., Vörösmarty, C. J., Fekete, B. M. & Peterson, B. J. 2001 Assessment of contemporary Arctic river runoff based on observational discharge record. *J. Geophys. Res.* **106** (D4), 3321–3334.

Lewis, T., Braun, C., Hardy, D. R., Francus, P. & Bradley, R. C. 2005 An extreme sediment transfer event in a Canadian High Arctic stream. *Arct. Antarct. Alp. Res.* **37** (4), 477–482.

Peart, M. R. & Walling, D. E. 1988 Techniques for establishing suspended sediment sources in two drainage basins in Devon, UK: a comparative assessment. In: IAHS Publ. 174, pp. 269–279.

Mimikou, M. 1982 An investigation of suspended sediment rating curves in western and northern Greece. *Hydrol. Sci. J.* **27** (3), 369–383.

Rannie, W. F. 1978 An approach to the prediction of suspended sediment rating curves. In: *Research in Fluvial Geomorphology* (R. Davidson-Arnott & W. Nickling, eds). Geo Abstracts, Norwich, UK, pp. 149–161.

Rodriguez-Blanco, M. L., Taboada-Castro, M. M. & Taboada-Castro, M. T. 2010a Sources and sediment yield from a rural catchment in humid temperate environment, northwest Spain. *Earth Surf. Proc. Land.* **35** (3), 272–277.

Rodriguez-Blanco, M. L., Taboada-Castro, M. M. & Taboada-Castro, M. T. 2010b Sediment and phosphorus loss in runoff from an agroforestry catchment, NW Spain. *Land Degrad. Dev.* **21** (2), 161–170.

Slattery, M. C., Gares, P. A. & Philips, J. D. 2002 Slope-channel linkage and sediment delivery on North Carolina Coastal Plain cropland. *Earth Surf. Proc. Land.* **27**, 1377–1387.

Syvitski, J. P. M., Morehead, M. D., Bahr, D. B. & Mulder, T. 2000 Estimating fluvial sediment transport: the rating parameters. *Water Resour. Res.* **36** (9), 2747–2760.

Tananaev, N. I. 2007a Using rating curve in estimation of suspended sediment flux from ungauged watersheds of North-Eastern Russia. In: *Proc. 10th International Symposium on River Sedimentation*, Moscow, Russia, 2007, Vol. III, pp. 314–321.

Tananaev, N. I. 2007b In: NGU Report 2007.050. Fourth Workshop of I.A.G./A.I.G. SEDIBUD, Trondheim, p. 33.

Tananaev, N. I. 2009 Impact of permafrost conditions on quantification of sediment fluxes and related channel type stability issues. In: NGU Report 2009.050. Fourth Workshop of I.A.G./A.I.G. SEDIBUD, Trondheim, p. 33.

Taylor, K. G., Owens, P. N., Batalla, R. J. & Garcia, C. 2008 Sediment and contaminant sources and transfers in river basins. In: *Sustainable Management of Sediment Resources*. Vol. 4 (P. N. Owens, ed.). Elsevier, Amsterdam, pp. 83–135.

Van Vliet-Lanoë, B., Coutard, J.-P. & Pissart, A. 1984 Structures caused by repeated freezing and thawing in various loamy

sediment: A comparison of active, fossil and experimental data. *Earth Surf. Proc. Land.* **9** (6), 553–565.

Viers, J., Dupré, B. & Gaillardet, J. 2009 Chemical composition of suspended sediment in World Rivers: New insights from a new database. *Sci. Total Environ.* **407**, 853–868.

Walling, D. E. 1977 Assessing the accuracy of suspended sediment rating curve for a small basin. *Water Resour. Res.* **13** (3), 531–537.

Walling, D. E. & Webb, B. W. 1982 Sediment availability and the prediction of storm-period sediment yield. In: IAHS Publ. 137, pp. 327–337.

Williams, G. P. 1989 Sediment concentration versus water discharge during single hydrologic events in rivers. *J. Hydrol.* **111**, 89–106.

Wood, P. A. 1977 Controls of variation in suspended sediment concentration in the river Rother, West Sussex, UK. *Sedimentology* **24**, 437–445.

First received 22 December 2011; accepted in revised form 11 September 2013. Available online 8 October 2013